Arch Appl Mech (2017) 87:201–217
DOI 10.1007/s00419-016-1187-8

ORIGINAL

Jianbin Chen · Qihong Fang · Jianke Du · Chao Xie · Feng Liu

Impact of process parameters on subsurface crack growth in brittle materials grinding

Received: 23 April 2016 / Accepted: 27 September 2016 / Published online: 13 October 2016

Abstract The main failure mechanism of brittle materials occurs through the initiation and propagation of cracks. Researches involved with various loading modes and material defects have been widely investigated to control the stability of subsurface crack. However, no detailed fracture mechanics analysis has been published to understand the direct effect of process parameters on crack growth. In this paper, taking the plastic deformation below the tool and the intrinsic line defect located at the plastic zone boundary into account, a mechanical and numerical study of the fracture mechanics is proposed from the perspective of process parameters in grinding of brittle materials. The stress intensity factors are computed in detail to analyze the various impacts of process parameters and tool geometry on the subsurface crack propagation. Results indicate that the main fracture mode for median crack induced in brittle material grinding is opening rather than shear. Although the residual stress caused by plastic zone plays an important role in fracture behavior, the effect of dislocations cannot be ignored as well. In addition, the starting point of opening fracture is also affected by grinding parameters and tool geometry. A small grinding speed, a sharp large tool, a large table speed and grinding depth will lead to strong anti-shielding effect on mode I crack propagation and strong shielding effect on mode II crack propagation. The results can be used to provide guidance for the development of controlled spalling technology which enables the reuse of cracking substrate.

Keywords Brittle materials · Grinding parameters · Subsurface crack growth · Stress intensity factor

1 Introduction

Brittle materials such as silicon, ceramic and glass are the most employed materials utilized in the manufacturing of a vast majority of semiconductor products, optical instruments, biological materials and various other fields [1–4]. However, brittle materials are not amenable to machining process due to their low fracture toughness.

J. Chen (✉) · J. Du · C. Xie
Piezoelectric Device Laboratory, Faculty of Mechanical Engineering and Mechanics, Ningbo University, Ningbo 315211, Zhejiang Province, People's Republic of China
E-mail: chenjianbin@nbu.edu.cn

J. Chen · Q. Fang (✉)
State Key Laboratory of Advanced Design and Manufacturing for Vehicle Body, Hunan University, Changsha 410082, Hunan Province, People's Republic of China
E-mail: fangqh1327@hnu.edu.cn

F. Liu
State Key Laboratory of Powder Metallurgy, Central South University, Changsha 410083, Hunan Province, People's Republic of China

When a brittle material is loaded to the limit of its strength, it tends to undergo cleavage-based fracture in a macroscale machining process and finally fails by the nucleation and propagation of a crack resulting in damaged and non-transparent machined surface [5]. These damages may seriously alter the surface properties and cause strength degradation or even a catastrophic failure of brittle materials [6]. As a consequence, the investigation of growth of surface and subsurface cracks plays an important role in the evaluation of the machining of brittle materials.

In fact, quite a few researches in crack propagation under different loading modes have been carried out. Early in 1964, Cook et al. [7] computed the stress distribution close to crack tip with a finite tip radius which could be opened by means of a remotely applied tension field or a concentrated force, etc. It is concluded that inside a brittle solid, if a plane of weakness or potential cleavage was present and was roughly normal to the plane of the original crack, this interface might break and produce a secondary crack in such a manner as to interfere with the progress of the primary crack. Hillberry et al. [8] described an idea on how to control the propagation of a crack in crystalline materials to produce thin wafers in their patent. Ewart and Suresh [9] studied the crack propagation in ceramics under cyclic loads. Xu and Needleman [10] numerically analyzed the dynamic crack growth in brittle solids with an initial central crack subjected to tensile loading. Gao et al. [11] studied the mechanisms of intersonic shear crack propagation along a weak interface under shear dominated loading by both molecular dynamics and continuum elastodynamics. Promising results were presented for the simulation of crack propagation in single crystals under monotonic loading by Aslan et al. [12]. Bouchard et al. [13] presented a mechanical and numerical study of the fracture process through a detailed analysis of stress intensity factors (SIFs). Influences of process variables on crack propagation direction were elucidated in their study. Yu et al. [14–16] investigated the dynamic responses and fracture behavior of various structural members under impulsive loading. Additionally, Comninou et al. [17,18] have done many works on the propagation of subsurface crack subjected to surface force utilizing the distribution dislocation technique.

It has long been known that the presence of material defects such as impurities, vacancies, dislocations and microcracks can strongly influence the initiation and propagation of cracks [19–21]. In particular, the availability of dislocations in a material has a strong impact on fracture toughness. Lawn [22] mentioned that a propagating crack might activate pre-existing dislocation sources. Rice and Thomson [23] instituted a physical modeling to study the competition between dislocation emission and cleavage decohesion by comparing the load required to propagate a given crack with the load necessary to emit a dislocation on a slip plane inclined to the crack plane and intersecting the crack front. Renormalized molecular dynamics simulation of machining defect-free monocrystal silicon was carried out to investigate crack initiation process by Inamura et al. [24]. In their study, the generation of dislocation was observed and believed to play an important role in crack initiation process. Beltz et al. [25] and Fischer and Beltz [26] studied the role of crack blunting in the favorability of crack propagation versus dislocation emission using continuum concepts. The growth of a plane strain crack subjected to remote mode I cyclic loading under small-scale yielding was carried out by Deshpande et al. [27] and Clevering et al. [28] using discrete dislocation dynamics. Results showed that the resistance to crack growth tended to increase with an increasing density of dislocation sources. Investigations that aimed to describe the origin of fracture surface instabilities in brittle crystals containing intrinsic line defects in the form of dislocations were presented by Sherman et al. [29]. Sen et al. [30] reported an atomistic-level study of crack-tip cleavage to dislocation emission transition in silicon single crystals. Molecular dynamics simulations of crack propagation in the presence of defects in brittle crystalline materials under mode I loading were carried out by Petucci et al. [21]. Results indicated that the critical load was dependent on the defect species, geometry and position. Additionally, Zhou et al. [31–33] and Fang et al. [34–36] have done a great deal of successful works on the interaction between material defects and cracks as well. The solutions may have potentially significant application in addressing challenging material science, in particular their wear and contact fatigue analysis.

It is worth mentioning that observations of a small amount of plastic deformation in brittle materials have been reported in wear or abrasive machining studies [37–39]. As suggested by Lawn et al. [40], the subsurface cracks might also develop from the boundary zone between plastic and elastic deformation. Nakamura et al. [41] detected experimentally that the ductile–brittle transition point determined by subsurface cracks was shallower than that by surface cracks. Yan et al. [42] investigated the microscopic material removal mechanism of reaction-bonded silicon carbide through diamond turning experiments. Raman spectroscopy revealed that the ductile response of the workpiece material originated from the dislocation-based plasticity of 6H–SiC. Venkatachalam et al. [3] studied the transition undeformed chip thickness in micromachining of single-crystal brittle materials. In their research, the beginning of the formation and propagation of cracks were evaluated utilizing Irwin's model which gave the relation between the stress intensity factor (SIF) and applied normal

stress including effects of crack size and crack inclination. Wang et al. [43] studied the brittle–ductile transition mechanism involved in ultra-precision turning of silicon and pointed out that the deformation behavior of silicon under cutting force was an interaction between crack propagation and dislocation movement. Kharin et al. [44] developed an improved theoretical model of dislocational crack nucleation and growth in solids and analyzed the ductile/brittle behavior. In order to build up a fracture theory which describes the plastic deformation based on the behavior of various defects near the crack tip, the elastic interaction between defects and elliptical blunt cracks has prompted many investigations [45–47]. Recently, Fang and Zhang [48,49] have established a new analytical model considering the phase transformation in determining the normal threshold load that caused the emission of partial dislocations in silicon during nanoindentation and nanoscratching.

As mentioned above, the main failure mechanism of brittle materials occurs through the creation and propagation of cracks. Researches involved with various loading modes and material defects have been widely investigated to control the crack stability. However, no detailed fracture mechanics analysis has been published to understand the direct effect of process parameters on crack propagation in brittle materials grinding. As a significance material that drives the semiconductor and information technology industries, there is no doubt that the failure components made of silicon has become an important issue [50,51]. In this paper, a mechanical and numerical study of the fracture mechanics is presented from the perspective of process parameters in grinding of crystalline silicon. Stress fields caused by local plastic deformation and edge dislocation are both taken into account. The effects of different process parameters and tool geometry on crack propagation can be obtained rapidly through a detailed analysis of stress intensity factors.

2 Modeling

The physical problem to be investigated in the current work is depicted in Fig. 1. During brittle materials grinding, a plastic deformation zone with a depth d generates below the indenter. Generally speaking, the plastic zone is determined by material properties, normal force P and indenter geometry. While brittle mode serving as the dominant mode of material removal, median cracking which is considered as the main type of subsurface cracking nucleates and propagates downward along the load axis from the plastic deformation boundary. According to Fang and Zhang [48], we assume that an edge dislocation with Burgers vector $\vec{b}$ is located at the plastic zone boundary in silicon substrate ($b = a/\sqrt{6}$, a is the lattice parameter). The initial position and glide plane of edge dislocation are represented by α_d and β, respectively. The normal force P and the tangential force Q are imposed simultaneously on the specimen surface. Note that the edge dislocation can emit into the elastic matrix when the force acting on it reaches a critical value [36] and the median crack will be initiated only if the normal load is above a threshold value [52].

Various theoretical equations [53–55] have been proposed to evaluate the plastic zone size and subsurface crack, respectively. In the following study, we suppose that the median crack is well developed, that is to say, the median crack is larger than the plastic zone. Considering the threshold parameters (critical loading and its corresponding critical crack) obtained by Lawn and Evans [53], in brittle materials machining, the plastic zone and median crack are given as [56]:

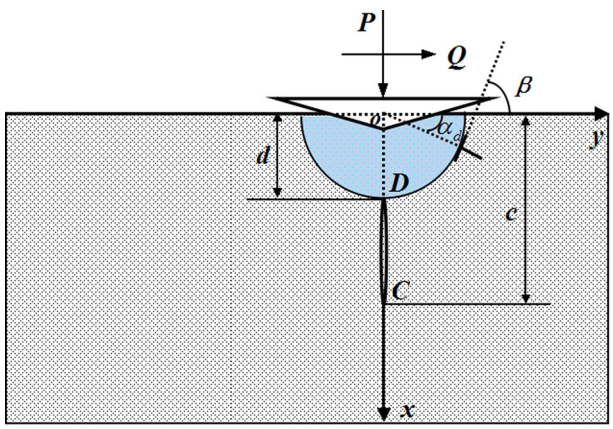

Fig. 1 Description of median crack propagation in brittle crystal materials grinding

Table 1 Material and geometric parameters in calculation

Young's modulus E (GPa)	Poisson's ratio υ	Hardness H (GPa)	Fracture toughness K_c (MPa · $m^{0.5}$)	Lattice parameter a (nm)	Slip plane β (deg)	α	η	χ_e	χ_r
168	0.27	10	0.6	0.542	54	$\frac{2}{\pi}$	1	0.038	0.026

$$d = \sqrt{\frac{\eta^2 P}{\alpha \pi H}} \tag{1}$$

$$c = \left[\frac{(\chi_e + \chi_r)\, P}{K_c}\right]^{2/3} \tag{2a}$$

$$\chi_r = \wp_r(\phi)\,(E/H)^{1-m}\,(\cot\alpha_i)^{2/3} \tag{2b}$$

$$\chi_e = \wp_e(\phi)\ln(2c/d) \tag{2c}$$

where E is the Young's modulus, H is the hardness, K_c is the fracture toughness, and α_i is the half apex angle of indenter. The dimensionless factors α and η are determined by indenter geometry, and the other two dimensionless terms $\wp_e(\phi)$ and $\wp_r(\phi)$ are dimensionless terms independent of the indenter/specimen system. The special values of indenter/specimen system parameters χ_e and χ_r for silicon have also been given by Lawn et al. [56] in their study as illustrated in Table 1.

Firstly, we consider the stress field induced in the material in the absence of the crack. Denote the normal and shear stresses along the line of the crack are $\tilde{\sigma}_{yy}$ and $\tilde{\sigma}_{xy}$, respectively, in the present case.

$$\tilde{\sigma}_{yy}(x,0) = \sigma_{yy\_s}(x,0) + \sigma_{yy\_r}(x,0) + \sigma_{yy\_d}(x,0), \quad d < x < c \tag{3}$$

$$\tilde{\sigma}_{xy}(x,0) = \sigma_{xy\_s}(x,0) + \sigma_{xy\_r}(x,0) + \sigma_{xy\_d}(x,0), \quad d < x < c \tag{4}$$

The stress components σ_{xy_s} and σ_{yy_s} caused by surface loading are written as [57]:

$$\sigma_{yy\_s}(x,0) = \frac{P(1-2\upsilon)}{4\pi x^2} \tag{5}$$

$$\sigma_{xy\_s}(x,0) = 0 \tag{6}$$

where υ is the Poisson's ratio.

The residual stresses σ_{xy_r} and σ_{yy_r} originated by the local inelastic deformation can be expressed as [58]:

$$\sigma_{yy\_r}(x,0) = \begin{cases} 0, & Q = 0 \\ \frac{4F_r\upsilon}{x^2}, & Q \neq 0 \end{cases} \tag{7}$$

$$\sigma_{yy\_r}(x,0) = \begin{cases} 0, & Q = 0 \\ -\frac{4F_r}{x^2}, & Q \neq 0 \end{cases} \tag{8}$$

The strength parameter F_r of residual stress field is determined by Jing et al. [55]

$$F_r = \frac{fE}{H}\frac{3P\lambda_r^2\cot\alpha_i}{4\pi^2(1-2\upsilon)(1+\upsilon)} \tag{9}$$

where f is the compaction factor ($fE/H = 1.09$ for sharp indenter) and λ_r is a dimensionless parameter determined by indenter geometry ($\lambda_r = 1.25$ for a Berkovich indenter).

By utilizing the distributed dislocation technique [59], the stress fields σ_{xy_d} and σ_{yy_d} due to the edge dislocation at position (x_0, y_0) with Burgers vector $\vec{b}$ are given as:

$$\sigma_{yy\_d}(x,0) = \frac{2\mu}{\pi(\kappa+1)}\left[b_x G_{xyy}(x,0;x_0,y_0) + b_y G_{yyy}(x,0;x_0,y_0)\right] \tag{10}$$

$$\sigma_{xy\_d}(x,0) = \frac{2\mu}{\pi(\kappa+1)}\left[b_x G_{xyx}(x,0;x_0,y_0) + b_y G_{yyx}(x,0;x_0,y_0)\right] \tag{11}$$

where

$$
\begin{aligned}
b_x &= b\sin\beta \\
b_y &= b\cos\beta \\
\kappa &= 3-4\upsilon \\
G_{xyy}(x,0;x_0,y_0) &= \frac{-y_0}{\left[(x-x_0)^2+y_0^2\right]^2}\left[(x-x_0)^2-y_0^2\right] \\
&\quad -\frac{4x_0y_0}{\left[(x+x_0)^2+y_0^2\right]^2}\left[(3x+2x_0)-\frac{4x\,(x+x_0)^2}{(x+x_0)^2+y_0^2}\right] \\
&\quad +\frac{y_0}{(x+x_0)^2+y_0^2}\left[\frac{2\,(x+x_0)^2}{(x+x_0)^2+y_0^2}-1\right] \\
G_{xxy}(x,0;x_0,y_0) &= \frac{x-x_0}{\left[(x-x_0)^2+y_0^2\right]^2}\left[(x-x_0)^2-y_0^2\right] \\
&\quad +\frac{4x_0\,(x+x_0)}{\left[(x+x_0)^2+y_0^2\right]^2}\left[(4x+x_0)-\frac{4x\,(x+x_0)^2}{(x+x_0)^2+y_0^2}\right] \\
&\quad +\frac{x+x_0}{(x+x_0)^2+y_0^2}\left[\frac{2\,(x+x_0)^2}{(x+x_0)^2+y_0^2}-1\right]-\frac{2x_0}{(x+x_0)^2+y_0^2} \\
G_{yyy}(x,0;x_0,y_0) &= \frac{x-x_0}{\left[(x-x_0)^2+y_0^2\right]^2}\left[(x-x_0)^2+3y_0^2\right] \\
&\quad +\frac{4x_0\,(x+x_0)}{\left[(x+x_0)^2+y_0^2\right]^2}\left[(4x+x_0)-\frac{4x\,(x+x_0)^2}{(x+x_0)^2+y_0^2}\right] \\
&\quad -\frac{x+x_0}{(x+x_0)^2+y_0^2}\left[\frac{2\,(x+x_0)^2}{(x+x_0)^2+y_0^2}-3\right]-\frac{2x_0}{(x+x_0)^2+y_0^2} \\
G_{yxy}(x,0;x_0,y_0) &= \frac{-y_0}{\left[(x-x_0)^2+y_0^2\right]^2}\left[(x-x_0)^2-y_0^2\right] \\
&\quad +\frac{4x_0y_0}{\left[(x+x_0)^2+y_0^2\right]^2}\left[x-\frac{4x\,(x+x_0)^2}{(x+x_0)^2+y_0^2}\right] \\
&\quad +\frac{y_0}{(x+x_0)^2+y_0^2}\left[\frac{2\,(x+x_0)^2}{(x+x_0)^2+y_0^2}-1\right]
\end{aligned}
$$

For the convenience of writing, we set

$$
\begin{aligned}
G_1(x) &= G_{xyy}(x,0;x_0,y_0),\ G_2(x) = G_{xxy}(x,0;x_0,y_0) \\
G_3(x) &= G_{yyy}(x,0;x_0,y_0),\ G_4(x) = G_{yxy}(x,0;x_0,y_0)
\end{aligned}
$$

It should be emphasized that four possible modes of response, i.e., open, closed and slipping forwards, closed and stuck, closed and slipping backwards, may well occur in combination for a given crack, sometimes at a given point in its history. The point $(x,0)$ at crack line is expected to be closed when the stress component $\tilde{\sigma}_{yy}(x,0)$ is compressive and only glide dislocations will be distributed along crack line. In contrast, the crack is expected to be open if $\tilde{\sigma}_{yy}(x,0)$ is tensile. In this case, climb dislocations must be distributed along the crack line and glide dislocations should be distributed as well if $\tilde{\sigma}_{xy}(x,0)\neq 0$. Therefore, in order to judge whether the median crack is open or closed in current state, influences of surface load on normal stress $\tilde{\sigma}_{yy}$ and shear stress $\tilde{\sigma}_{xy}$ along the imaginary crack line are shown in Fig. 2. Notice that both the plastic zone d and the median crack depth c changed with the normal force P, and therefore the horizontal axis in Fig. 2 has been

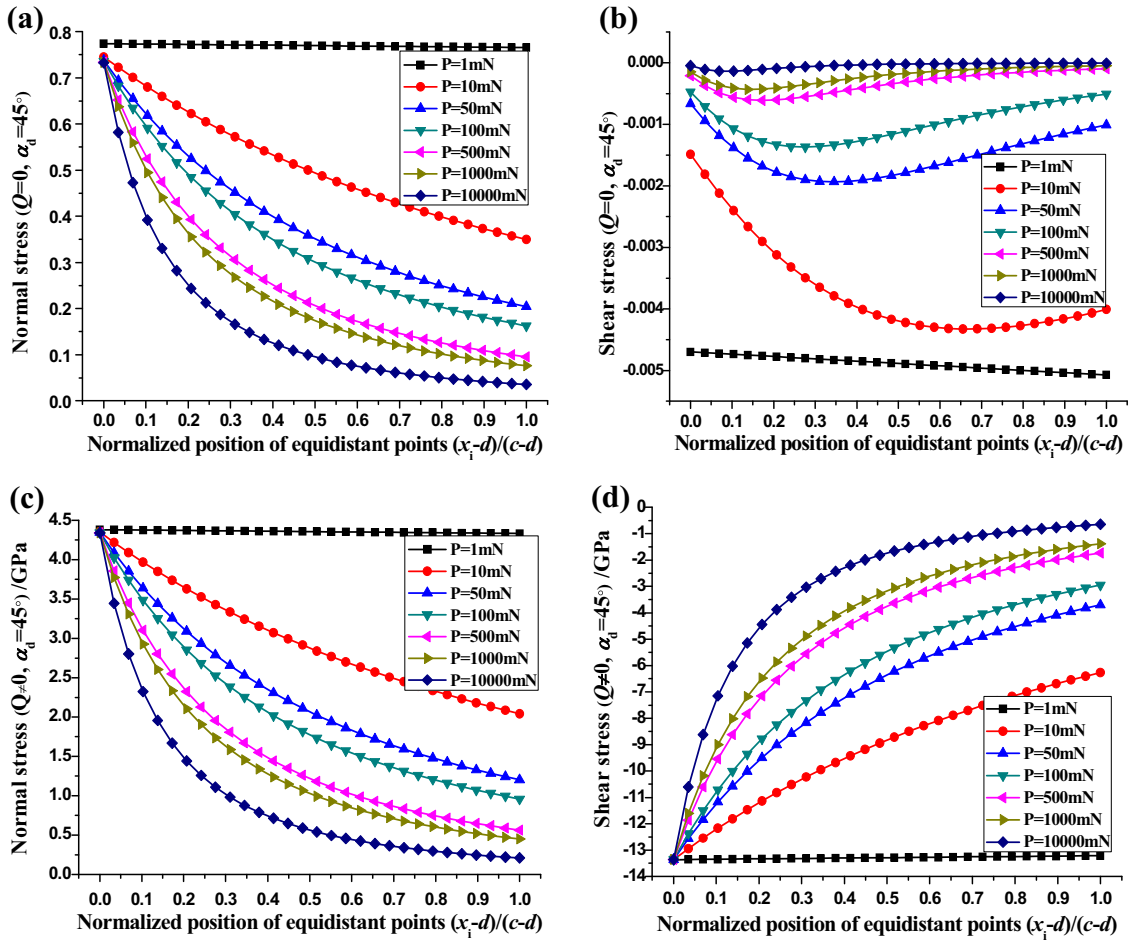

Fig. 2 Stress components generated in the imaginary crack line ($\alpha_d = 45°$)

replaced by a normalized position $(x_i - d)/(c - d)$ for comparison. In addition, the material and geometric parameters adapted in calculation are given in Table 1 [48,53,56].

It can be seen that if there is a lateral force (Fig. 2c, d) or not (Fig. 2a, b), the normal stress component is always positive which means the median crack is always open while the shear stress component is always negative. As a result, both climb dislocations and glide dislocations need distributing along the crack line. Besides, larger surface normal load corresponds to smaller normal stress and the tangential force can increase both the normal and shear stresses.

In the presence of median crack, the normal $N(x)$ and shear $S(x)$ tractions arising on the crack faces $(y = 0)$ can be expressed as [59]:

$$S(x) \equiv \tilde{\sigma}_{xy}(x, 0) + \bar{\sigma}_{xy}(x, 0), \quad d < x < c \tag{12}$$

$$N(x) \equiv \tilde{\sigma}_{yy}(x, 0) + \bar{\sigma}_{yy}(x, 0), \quad d < x < c \tag{13}$$

The corrective solutions $\bar{\sigma}_{xy}(x, 0)$ and $\bar{\sigma}_{yy}(x, 0)$ due to the crack can be obtained as distributions of edge dislocations.

$$\bar{\sigma}_{xy}(x, 0) = \frac{2\mu}{\pi(\kappa + 1)} \int_c^d \left[\frac{1}{x - \xi} + K(x, \xi)\right] B_x(\xi)\, \mathrm{d}\xi \tag{14}$$

$$\bar{\sigma}_{yy}(x, 0) = \frac{2\mu}{\pi(\kappa + 1)} \int_d^c \left[\frac{1}{x - \xi} + K(x, \xi)\right] B_y(\xi) \mathrm{d}\xi \tag{15}$$

where $K(x,\xi) = -\frac{1}{x+\xi} - \frac{2\xi}{(x+\xi)^2} + \frac{4\xi^2}{(x+\xi)^3}$, $B_x(\xi)$ and $B_y(\xi)$ are the density of glide and climb dislocations at point $(\xi, 0)$, respectively. The integration limits in Eqs. (14) and (15) are controlled by the plastic zone and the median crack depth depending on normal force P as expressed in Eqs. (1) and (2).

According to the definition of stress intensity factor, the Mode I and Mode II SIFs at crack tips D and C are

$$K_{\mathrm{I}}(D) = -\lim_{x\to d}\left\{\frac{2\mu}{(\kappa+1)}B_y(x)\sqrt{2\pi(x-d)}\right\} \tag{16}$$

$$K_{\mathrm{I}}(C) = -\lim_{x\to c}\left\{\frac{2\mu}{(\kappa+1)}B_y(x)\sqrt{2\pi(c-x)}\right\} \tag{17}$$

$$K_{\mathrm{II}}(D) = -\lim_{x\to d}\left\{\frac{2\mu}{(\kappa+1)}B_x(x)\sqrt{2\pi(x-d)}\right\} \tag{18}$$

$$K_{\mathrm{II}}(C) = \lim_{x\to c}\left\{\frac{2\mu}{(\kappa+1)}B_x(x)\sqrt{2\pi(c-x)}\right\} \tag{19}$$

Substituting Eqs. (14), (15) into Eqs. (12), (13) yields

$$S(x) = \begin{cases} \frac{2\mu}{\pi(\kappa+1)}\left[b_x G_2(x) + b_y G_4(x) + \int_d^c\left(\frac{1}{x-\xi} + K(x,\xi)\right)B_x(\xi)\,\mathrm{d}\xi\right], & Q = 0 \\ -\frac{4F_r}{x^2} + \frac{2\mu}{\pi(\kappa+1)}\left[b_x G_2(x) + b_y G_4(x) + \int_d^c\left(\frac{1}{x-\xi} + K(x,\xi)\right)B_x(\xi)\,\mathrm{d}\xi\right], & Q \neq 0 \end{cases} \tag{20}$$

$$N(x) = \begin{cases} \frac{P(1-2\upsilon)}{4\pi x^2} + \frac{2\mu}{\pi(\kappa+1)}\left[b_x G_1(x) + b_y G_3(x) + \int_d^c\left(\frac{1}{x-\xi} + K(x,\xi)\right)B_y(\xi)\,\mathrm{d}\xi\right], & Q = 0 \\ \frac{P(1-2\upsilon)}{4\pi x^2} + \frac{4F_r\upsilon}{x^2} + \frac{2\mu}{\pi(\kappa+1)}\left[b_x G_1(x) + b_y G_3(x) + \int_d^c\left(\frac{1}{x-\xi} + K(x,\xi)\right)B_y(\xi)\,\mathrm{d}\xi\right], & Q \neq 0 \end{cases} \tag{21}$$

When the crack is open at all points, the requirement that the crack faces holds traction-free is

$$N(x) = S(x) = 0 \quad , d \le x \le c \tag{22}$$

Then Eqs. (20), (21) can be rewritten as:

$$\frac{1}{\pi}\int_d^c\left[\frac{1}{x-\xi} + K'(x,\xi)\right]B_x(\xi)\,\mathrm{d}\xi = \begin{cases} -\frac{1}{\pi}\left[b_x G_2(x) + b_y G_4(x)\right], & Q = 0 \\ -\frac{1}{\pi}\left[b_x G_2(x) + b_y G_4(x)\right] + \frac{2F_r(\kappa+1)}{\mu x^2}, & Q \neq 0 \end{cases} \tag{23}$$

$$\frac{1}{\pi}\int_d^c\left[\frac{1}{x-\xi} + K(x,\xi)\right]B_y(\xi)\,\mathrm{d}\xi = \begin{cases} -\frac{b_x G_1(x)+b_y G_3(x)}{\pi} - \frac{P(1-2\upsilon)(\kappa+1)}{8\mu\pi x^2}, & Q = 0 \\ -\frac{b_x G_1(x)+b_y G_3(x)}{\pi} - \frac{[P(1-2\upsilon)+16\pi F_r\upsilon](\kappa+1)}{8\mu\pi x^2}, & Q \neq 0 \end{cases} \tag{24}$$

Notice that these two equations give rise to two uncoupled integral equations as for a crack normal to the surface of a half-plane.

In addition, due to the uniqueness of displacements, two further equations are needed to render the problem determinate.

$$\int_d^c B_x(\xi)\,\mathrm{d}\xi = 0 \tag{25}$$

$$\int_d^c B_y(\xi)\,\mathrm{d}\xi = 0 \tag{26}$$

3 Numerical solutions

As the presence of the Cauchy integral in Eqs. (23) and (24), firstly, the interval of integration (d, c) is normalized by the change of variables

$$x = \delta s + \rho, \quad \xi = \delta r + \rho \tag{27}$$

where

$$\delta = \frac{c-d}{2}, \quad \rho = \frac{c+d}{2}, \quad |s| < 1, \quad |r| \leq 1 \tag{28}$$

Substituting Eqs. (27), (28) into Eqs. (23), (24) yields

$$\frac{1}{\pi}\int_{-1}^{+1}\left[\frac{1}{s-r}+\delta K'(s,r)\right]B_x(r)\,\mathrm{d}r = \begin{cases} -\frac{1}{\pi}\left[b_x G_2'(s)+b_y G_4'(s)\right], & Q=0 \\ -\frac{1}{\pi}\left[b_x G_2'(s)+b_y G_4'(s)\right]+\frac{2F_r(\kappa+1)}{\mu(\delta s+\rho)^2}, & Q\neq 0 \end{cases} \tag{29}$$

$$\frac{1}{\pi}\int_{-1}^{+1}\left[\frac{1}{s-r}+\delta K'(s,r)\right]B_y(r)\,\mathrm{d}r = \begin{cases} -\frac{b_x G_1'(s)+b_y G_3'(s)}{\pi}-\frac{P(1-2\upsilon)(\kappa+1)}{8\mu\pi(\delta s+\rho)^2}, & Q=0 \\ -\frac{b_x G_1'(s)+b_y G_3'(s)}{\pi}-\frac{[P(1-2\upsilon)+16\pi F_r\upsilon](\kappa+1)}{8\mu\pi(\delta s+\rho)^2}, & Q\neq 0 \end{cases} \tag{30}$$

where

$$\begin{aligned}
G_1'(s) &= \frac{-y_0\left[(\delta s+\rho-x_0)^2-y_0^2\right]}{\left[(\delta s+\rho-x_0)^2+y_0^2\right]^2}-\frac{4x_0y_0\left\{[2x_0-(\delta s+\rho)]\,(\delta s+\rho+x_0)^2+[3(\delta s+\rho)+2x_0]\,y_0^2\right\}}{\left[(\delta s+\rho+x_0)^2+y_0^2\right]^3} \\
&\quad+\frac{y_0\left[(\delta s+\rho+x_0)^2-y_0^2\right]}{\left[(\delta s+\rho+x_0)^2+y_0^2\right]^2} \\
G_2'(s) &= \frac{(\delta s+\rho-x_0)\left[(\delta s+\rho-x_0)^2-y_0^2\right]}{\left[(\delta s+\rho-x_0)^2+y_0^2\right]^2}+\frac{4x_0(\delta s+\rho+x_0)\left\{x_0(\delta s+\rho+x_0)^2+[4(\delta s+\rho)+x_0]\,y_0^2\right\}}{\left[(\delta s+\rho+x_0)^2+y_0^2\right]^3} \\
&\quad+\frac{(\delta s+\rho+x_0)\left[(\delta s+\rho+x_0)^2-y_0^2\right]}{\left[(\delta s+\rho+x_0)^2+y_0^2\right]^2}-\frac{2x_0}{(\delta s+\rho+x_0)^2+y_0^2} \\
G_3'(s) &= \frac{(\delta s+\rho-x_0)\left[(\delta s+\rho-x_0)^2+3y_0^2\right]}{\left[(\delta s+\rho-x_0)^2+y_0^2\right]^2}+\frac{4x_0(\delta s+\rho+x_0)\left\{x_0(\delta s+\rho+x_0)^2+[4(\delta s+\rho)+x_0]\,y_0^2\right\}}{\left[(\delta s+\rho+x_0)^2+y_0^2\right]^3} \\
&\quad+\frac{(\delta s+\rho+x_0)\left[(\delta s+\rho+x_0)^2+3y_0^2\right]}{\left[(\delta s+\rho+x_0)^2+y_0^2\right]^2}-\frac{2x_0}{(\delta s+\rho+x_0)^2+y_0^2} \\
G_4'(s) &= \frac{-y_0\left[(\delta s+\rho-x_0)^2-y_0^2\right]}{\left[(\delta s+\rho-x_0)^2+y_0^2\right]^2}+\frac{y_0\left[(\delta s+\rho+x_0)^2-y_0^2\right]}{\left[(\delta s+\rho+x_0)^2+y_0^2\right]^2}+\frac{4x_0y_0(\delta s+\rho)\left[y_0^2-3(\delta s+\rho+x_0)^2\right]}{\left[(\delta s+\rho+x_0)^2+y_0^2\right]^3} \\
K'(s,r) &= -\frac{1}{\delta(s+r)+2\rho}-\frac{2(\delta r+\rho)}{[\delta(s+r)+2\rho]^2}+\frac{4(\delta r+\rho)^2}{[\delta(s+r)+2\rho]^3}
\end{aligned}$$

and Eqs. (25), (26) can be rewritten as:

$$\int_{-1}^{+1} B_x(r)\,\mathrm{d}r = 0 \tag{31}$$

$$\int_{-1}^{+1} B_y(r)\,\mathrm{d}r = 0 \tag{32}$$

For handling singular integral equations with Cauchy kernels, we follow the widely used Gauss–Chebyshev numerical quadrature developed by Erdogan and Gupta [60]. Since both B_x and B_y are bounded functions, we set

$$B_x(r) = w(r)\,\varphi_x(r) \tag{33}$$

$$B_y(r) = w(r)\,\varphi_y(r) \tag{34}$$

where the unknown $\varphi_x(r)$ and $\varphi_y(r)$ in the expressions of dislocation density are some smooth regular functions.

In current case, both the crack tips are singular. The corresponding fundamental function $w(r)$ has been given by Dundurs and Comninou [61].

$$w(r) = \left(1-r^2\right)^{-1/2} \tag{35}$$

Finally, the discrete forms of Eqs. (29) and (30) become

$$\sum_{i=1}^{n} W_i \varphi_x(r_i)\left[\frac{1}{s_k - r_i} + \delta K'(s_k, r_i)\right] = \begin{cases} -\frac{1}{\pi}\left[b_x G_2'(s_k) + b_y G_4'(s_k)\right], & Q = 0 \\ -\frac{1}{\pi}\left[b_x G_4'(s_k) + b_y G_4'(s_k)\right] + \frac{2F_r(\kappa+1)}{\mu(\delta s_k+\rho)^2}, & Q \neq 0 \end{cases} \quad k = 1, \ldots, n-1 \tag{36}$$

$$\sum_{i=1}^{n} W_i \varphi_y(r_i)\left[\frac{1}{s_k - r_i} + \delta K'(s_k, r_i)\right] = \begin{cases} -\frac{b_x G_1'(s_k)+b_y G_3'(s_k)}{\pi} - \frac{P(1-2\upsilon)(\kappa+1)}{8\mu\pi(\delta s_k+\rho)^2}, & Q = 0 \\ -\frac{b_x G_1'(s_k)+b_y G_3'(s_k)}{\pi} - \frac{[P(1-2\upsilon)+16\pi F_r \upsilon](\kappa+1)}{8\mu\pi(\delta s_k+\rho)^2}, & Q \neq 0 \end{cases} \quad k = 1, \ldots, n-1 \tag{37}$$

$$\sum_{i=1}^{n} \frac{\varphi_x(r_i)}{n} = 0 \tag{38}$$

$$\sum_{i=1}^{n} \frac{\varphi_y(r_i)}{n} = 0 \tag{39}$$

where

$$r_i = \cos\left(\frac{2i-1}{2n}\pi\right), \quad i = 1, \ldots, n$$

$$s_k = \cos\left(\frac{k}{n}\pi\right), \quad k = 1, \ldots, n-1$$

$$W_i = \frac{1}{n}$$

$$G_1'(s_k) = \frac{-y_0\left[(\delta s_k+\rho-x_0)^2 - y_0^2\right]}{\left[(\delta s_k+\rho-x_0)^2 + y_0^2\right]^2} - \frac{4x_0 y_0\left\{[2x_0 - (\delta s_k+\rho)]\,(\delta s_k+\rho+x_0)^2 + [3(\delta s_k+\rho)+2x_0]\,y_0^2\right\}}{\left[(\delta s_k+\rho+x_0)^2 + y_0^2\right]^3} + \frac{y_0\left[(\delta s_k+\rho+x_0)^2 - y_0^2\right]}{\left[(\delta s_k+\rho+x_0)^2 + y_0^2\right]^2}$$

$$G_2'(s_k) = \frac{(\delta s_k+\rho-x_0)\left[(\delta s_k+\rho-x_0)^2 - y_0^2\right]}{\left[(\delta s_k+\rho-x_0)^2 + y_0^2\right]^2} + \frac{4x_0(\delta s_k+\rho+x_0)\left\{x_0(\delta s_k+\rho+x_0)^2 + [4(\delta s_k+\rho)+x_0]\,y_0^2\right\}}{\left[(\delta s_k+\rho+x_0)^2 + y_0^2\right]^3} + \frac{(\delta s_k+\rho+x_0)\left[(\delta s_k+\rho+x_0)^2 - y_0^2\right]}{\left[(\delta s_k+\rho+x_0)^2 + y_0^2\right]^2} - \frac{2x_0}{(\delta s_k+\rho+x_0)^2 + y_0^2}$$

$$G_3'(s_k) = \frac{(\delta s_k+\rho-x_0)\left[(\delta s_k+\rho-x_0)^2 + 3y_0^2\right]}{\left[(\delta s_k+\rho-x_0)^2 + y_0^2\right]^2} + \frac{4x_0(\delta s_k+\rho+x_0)\left\{x_0(\delta s_k+\rho+x_0)^2 + [4(\delta s_k+\rho)+x_0]\,y_0^2\right\}}{\left[(\delta s_k+\rho+x_0)^2 + y_0^2\right]^3} + \frac{(\delta s_k+\rho+x_0)\left[(\delta s_k+\rho+x_0)^2 + 3y_0^2\right]}{\left[(\delta s_k+\rho+x_0)^2 + y_0^2\right]^2} - \frac{2x_0}{(\delta s_k+\rho+x_0)^2 + y_0^2}$$

$$G_4'(s_k) = \frac{-y_0\left[(\delta s_k+\rho-x_0)^2 - y_0^2\right]}{\left[(\delta s_k+\rho-x_0)^2 + y_0^2\right]^2} + \frac{4x_0 y_0(\delta s_k+\rho)\left[y_0^2 - 3(\delta s_k+\rho+x_0)^2\right]}{\left[(\delta s_k+\rho+x_0)^2 + y_0^2\right]^3} + \frac{y_0\left[(\delta s_k+\rho+x_0)^2 - y_0^2\right]}{\left[(\delta s_k+\rho+x_0)^2 + y_0^2\right]^2}$$

And the stress intensity factors at crack tips are directly related to the regular functions $\varphi(r)$ at end points $r = \pm 1$ which can be determined as:

$$K_{\mathrm{I}}(\pm 1) = \pm\sqrt{\frac{\pi(c-d)}{2}}\frac{2\mu}{(\kappa+1)}\varphi_y(\pm 1) \tag{40}$$

$$K_{\mathrm{II}}(\pm 1) = \pm\sqrt{\frac{\pi(c-d)}{2}}\frac{2\mu}{(\kappa+1)}\varphi_x(\pm 1) \tag{41}$$

The expressions of $\varphi(\pm 1)$ are given as [59]:

$$\varphi(+1) = M_E(+1) \sum_{i=1}^{n} \Phi_E(+1)\varphi(r_i) \tag{42}$$

$$\varphi(-1) = M_E(-1) \sum_{i=1}^{n} \Phi_E(-1)\varphi(r_{n+1-i}) \tag{43}$$

where

$$M_E(+1) = M_E(-1) = \frac{1}{n}$$

$$\Phi_E(+1) = \Phi_E(-1) = \frac{\sin\left[\frac{(2i-1)(2n-1)\pi}{4n}\right]}{\sin\left(\frac{2i-1}{4n}\pi\right)}$$

Note that in the above equations, the negative sign refers to the shallower crack tip D, while the positive sign + refers to the deeper one C. Additionally, although the indexes for $\varphi(\pm 1)$ on the right side of Eqs. (41) and (42) are impossible, these two vitally important values can be obtained by the discrete set of points r_i from Krenk's interpolation formulae [62].

4 Results and discussion

The stress intensity factor can be used for determining whether the mode of material removal is plastic deformation or crack propagation along certain slip systems [2]. On the other hand, each machining method has its corresponding input parameters. For scratch test, the main input parameters are normal force P, lateral force Q and penetration depth h applied on indenter. Notice that there is no lateral force in indentation experiment. Therefore, the stress intensity factors at both the shallower and deeper median crack tip under scratch or indentation test can be directly obtained from Eqs. (40) and (41) based on the MATLAB procedure.

Figure 3 shows the variation of stress intensity factors at point C with different positions of edge dislocation located at plastic deformation boundary in the presence of lateral force. Results show that the main fracture mode is opening rather than shear as the mode I SIF is always positive, while the mode II SIF is always negative. By comparing the data in Fig. 3a, c, we also find that the mode I SIF is larger than the fracture toughness K_c when $P = 100$ mN which means that a large surface normal load can promote the growth of type I cracking. However, it makes the occurrence of mode II crack difficult as depicted in Fig. 3b, d. Besides, each curve has a maximum value when the edge dislocation coincides with the start point of median crack ($\alpha_d = 90°$). In the following analyses, we take $\alpha_d = 36°$ when the effect of edge dislocation is under consideration.

The influence of normal force on stress intensity factors at both the two crack tips are illustrated in Fig. 4. It is seen that, when the median crack is well developed, the mode I SIF at the shallower tip is always larger than the deeper one with a positive value whether there is a lateral force or not. It is worth mentioning that this result does not mean the propagation of shallower crack is easier. The reason is that the plastic zone expands with the increased surface normal load and finally engulfs the shallower crack tip as demonstrated in Eq. (1). In addition, the mode II SIFs are positive only when the lateral force is absent and two intersections occur when the normal force is close to 37.5 and 500 mN, respectively.

As the shallower crack tip will become engulfed with the increased normal force, we are more interested in the crack propagation behavior of the deeper one. By comparing the critical normal force when the fracture occurs with and without consideration of existence of tangential force Q (see Fig. 4b, a respectively), we find that the threshold in the absence of lateral force is much larger (350 mN) than that in the presence of lateral force (1.33 mN). It means that the residual stress caused by plastic zone plays an important role in fracture behavior. This is most probably because the residual stress induced by plastic deformation in the subsurface is tensile as mentioned in Chen et al. [63]. Moreover, the Mode II fracture toughness can be easily obtained according to Chang et al. [64], i.e., $K_{IIC} = \frac{\sqrt{3}}{2} K_{IC} = 0.52$. Therefore, we can conclude that the Mode II crack propagation never happens whether the tangential force exists or not from the stress intensity factor shown in Fig. 4c, d. In particular, the tangential force has a obvious shielding effect on Mode II crack growth.

It is generally known that dislocation pile-up or coalescence is one of the mechanisms leading to the crack nucleation. According to the typical crack systems in brittle materials machining mentioned by Chen et al.

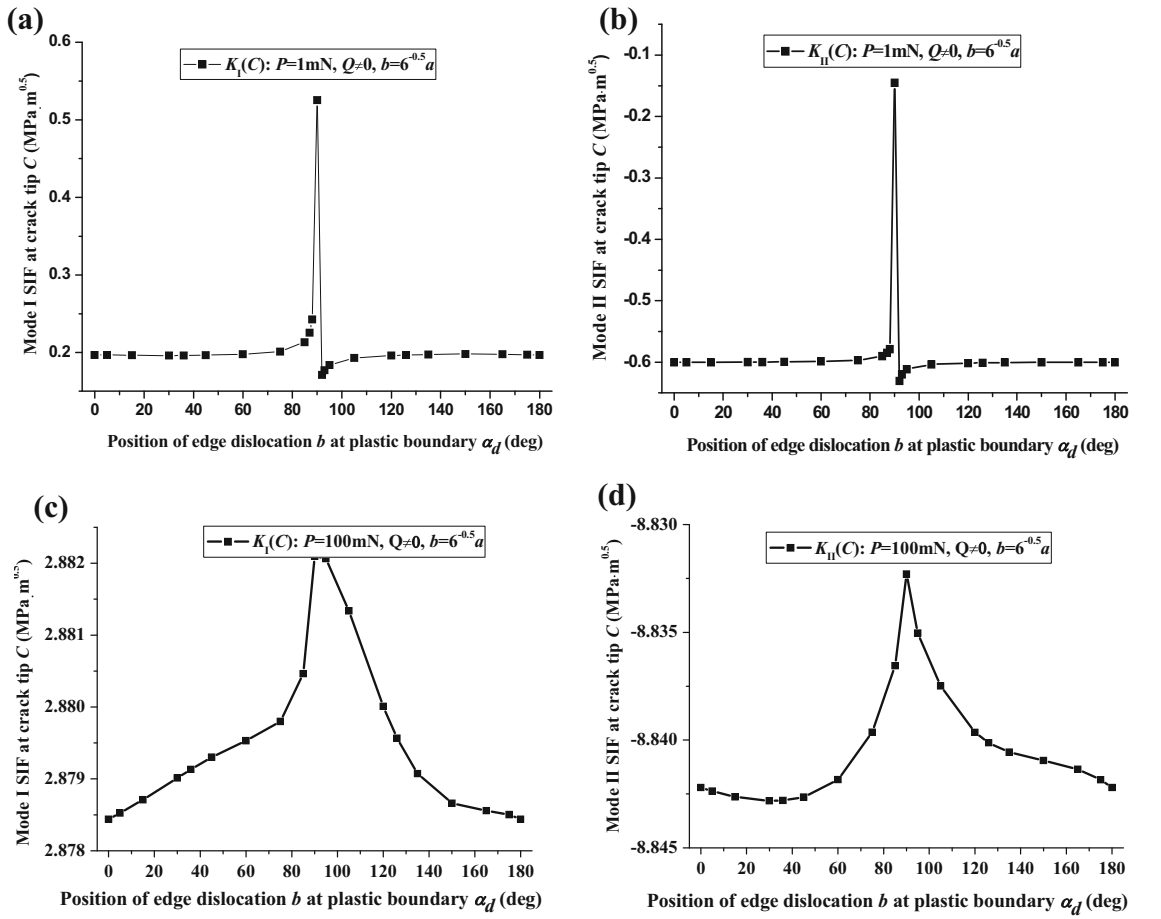

Fig. 3 Effects of various dislocation positions on stress intensity factors

[6], the median crack is the main type of subsurface damages. However, the lateral crack also initiates at or close to the boundary of the plastic zone and spreads out laterally on a plane closely parallel to the machined surface. Therefore, in this paper, an edge dislocation with specified location as discussed by Fang et al. [48] has been introduced before the lateral crack formation to investigate the interaction between median crack and dislocation. Figure 5a shows the proportion of stress intensity factors caused by dislocation in the absence of lateral force. Result indicates that the normal force P has no effect on mode II SIF. As illustrated in Fig. 5b, the percentage of mode II SIF caused by tangential force is above 100 % after considering the present of lateral force. That is to say, the dislocation generates a positive mode II SIF, while the lateral force induces a negative one. The total mode II SIF is caused by the combination of dislocation and residual stress. The proportion of mode I SIF caused by residual stress is nearly 83 % as depicted in Fig. 5b which reconfirms again the dominant role of plastic zone in growth of subsurface crack. In addition, a single edge dislocation can bring about 3 % of mode I SIF when normal force is close to 10 mN (see Fig. 5a). According to Yan et al. [65], the dislocation density depends on the machining conditions such as cutting depth and tool rake angle. A high dislocation density may exhibit around the potential crack. Therefore, the effect of dislocations on fracture behavior cannot be ignored in machining of brittle crystal materials. In the future work, the interaction between lateral crack and median crack can be further studied by utilizing the distributed dislocation technique as well.

When a component is processed by grinding, the main input parameters become wheel speed V_s, workpiece speed V_w and penetration depth h. As mentioned by Zhu et al. [66], median cracks could be effectively inhibited by moderate wheel speed. In order to quickly obtain the effect of various grinding parameters on subsurface crack propagation, we introduce the following equation established by Gu and Yao [67].

$$c_m = \lambda_c h_m^{4/3} \tag{44}$$

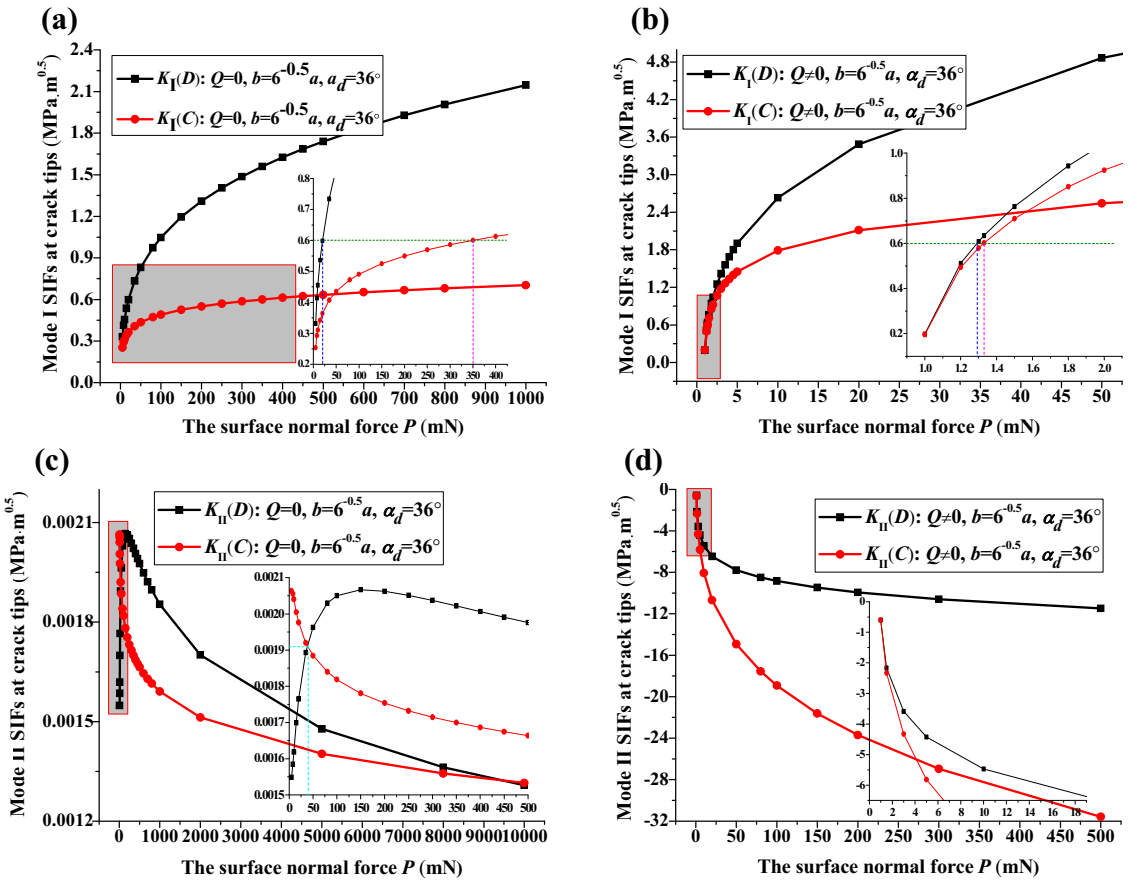

Fig. 4 Stress intensity factors under different loading conditions

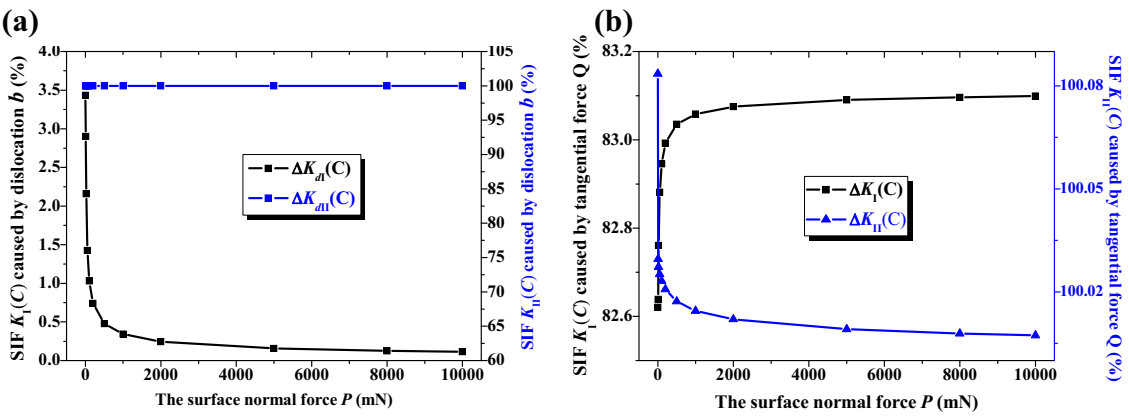

Fig. 5 The percentage of stress intensity factor caused by **a** dislocation, **b** residual stress

where $\lambda_c = 0.206(\mu H)^{1/3}/(K_c\beta_c)^{2/3}\,(\cot\alpha_i)^{4/9}\,(\tan\alpha_i)^{4/3}$, H is the hardness, K_c is the fracture toughness, and β_c is material parameter depended on elastic recovery.

The maximum penetration depth h_m was deduced by Shaw [68].

$$h_m = \left[\frac{4}{Ar_c}\frac{V_w}{V_s}\left(\frac{a_p}{d_e}\right)^{1/2}\right]^{1/2} \tag{45}$$

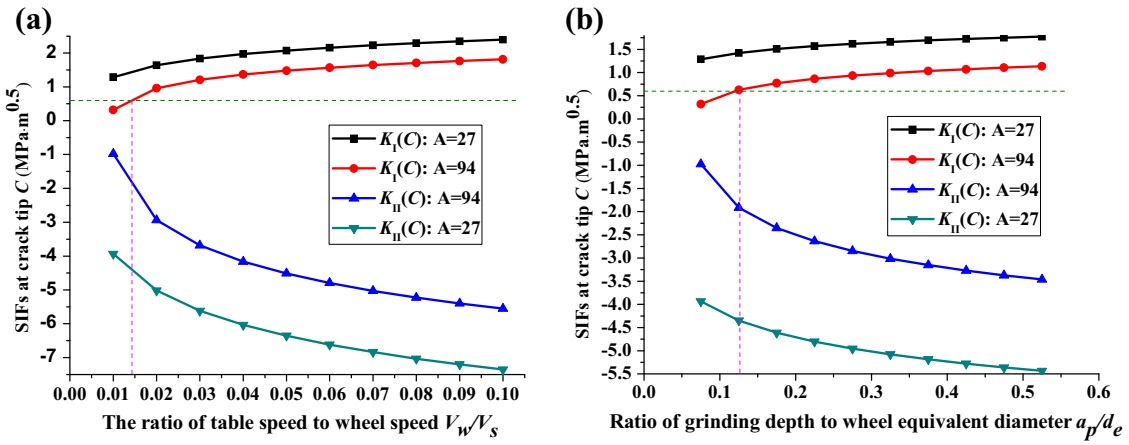

Fig. 6 The effect of grinding parameters on crack propagation

where r_c is the chip width-to-thickness ratio, A is the grain surface density (usually a large grain surface density corresponds to a small grit), a_p is the grinding depth, and d_e is the equivalent diameter of grinding wheel.

Then the median crack c_m can be expressed as a function of material properties, geometry of the abrasive grain and other grinding parameters by substituting Eqs. (45) into (44)

$$c_m = 0.206 \left[\frac{4}{Ar_c} \frac{V_w}{V_s} \left(\frac{a_p}{d_e} \right)^{1/2} \right]^{2/3} \left(\frac{\mu H}{K_c^2 \beta_c^2} \right)^{1/3} (\tan \alpha_i)^{8/9} \tag{46}$$

In the current situation, the normal grinding force P, the strength parameter of residual stress field F_r and the plastic zone size d can be rewritten as

$$P = \frac{0.0935 \left[\frac{4}{Ar_c} \frac{V_w}{V_s} \left(\frac{a_p}{d_e} \right)^{1/2} \right] (\mu H)^{1/2} (\tan \alpha_i)^{4/3}}{\beta_c (\chi_e + \chi_r)} \tag{47}$$

$$F_r = \frac{0.0764 \lambda_r^2 \left[\frac{4}{Ar_c} \frac{V_w}{V_s} \left(\frac{a_p}{d_e} \right)^{1/2} \right] (\mu H)^{1/2} (\tan \alpha_i)^{1/3}}{\pi^2 \beta_c (\chi_e + \chi_r)(1 - 2\upsilon)(1 + \upsilon)} \tag{48}$$

$$d = \frac{0.3058 \eta \left[\frac{4}{Ar} \frac{V_w}{V_s} \left(\frac{a_p}{d_e} \right)^{1/2} \right]^{1/2} \left(\frac{\mu}{H} \right)^{1/4} (\tan \alpha_i)^{2/3}}{[\alpha \beta_c \pi (\chi_e + \chi_r)]^{1/2}} \tag{49}$$

Finally, the effects of grinding parameters and abrasive grain geometry on crack propagation can be obtained by substituting Eqs. (47), (48) and (49) into Eqs. (40), (41). For convenience, we introduce two dimensionless parameters, i.e., the speed ratio r_s and the dimension ratio r_d.

$$r_s = \frac{V_w}{V_s}, \quad r_d = \frac{a_p}{d_e} \tag{50}$$

As shown in Figs. 6 and 7, the mode I SIF at crack tip C is always positive, while the mode II SIF is always negative. The large speed ratio and dimension ratio correspond to a large magnitude of SIF, while the blunt and small grit corresponds to a small magnitude. Results indicate that a small grinding speed, a sharp large tool, a large table speed and grinding depth will lead to strong anti-shielding effect on mode I crack propagation and strong shielding effect on mode II crack propagation. As a main fracture mode in brittle crystal materials grinding, the starting point of opening fracture is also affected by grinding parameters and tool geometry.

It is worth mentioning that the branch fracture will occur under the mixed-mode I/II loading conditions. Li et al. [69] stated that the angle between branches of brittle fracture was between 45° and 90° in most papers. Kozhushko et al. [70] observed the fracture behavior of silicon with mixed-mode loading, an angle of $\sim 70°$

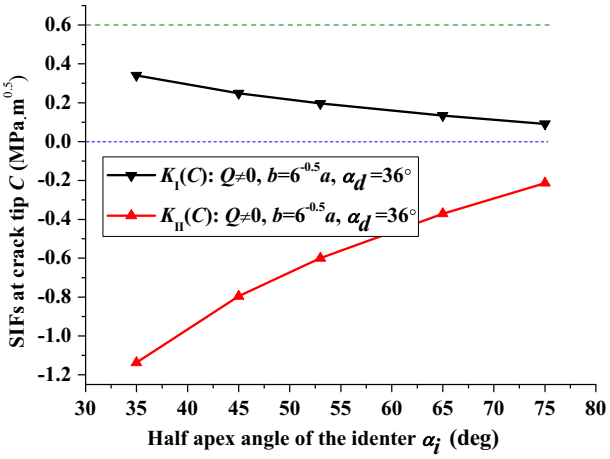

Fig. 7 The impact of grain's apex angle on growth of median crack

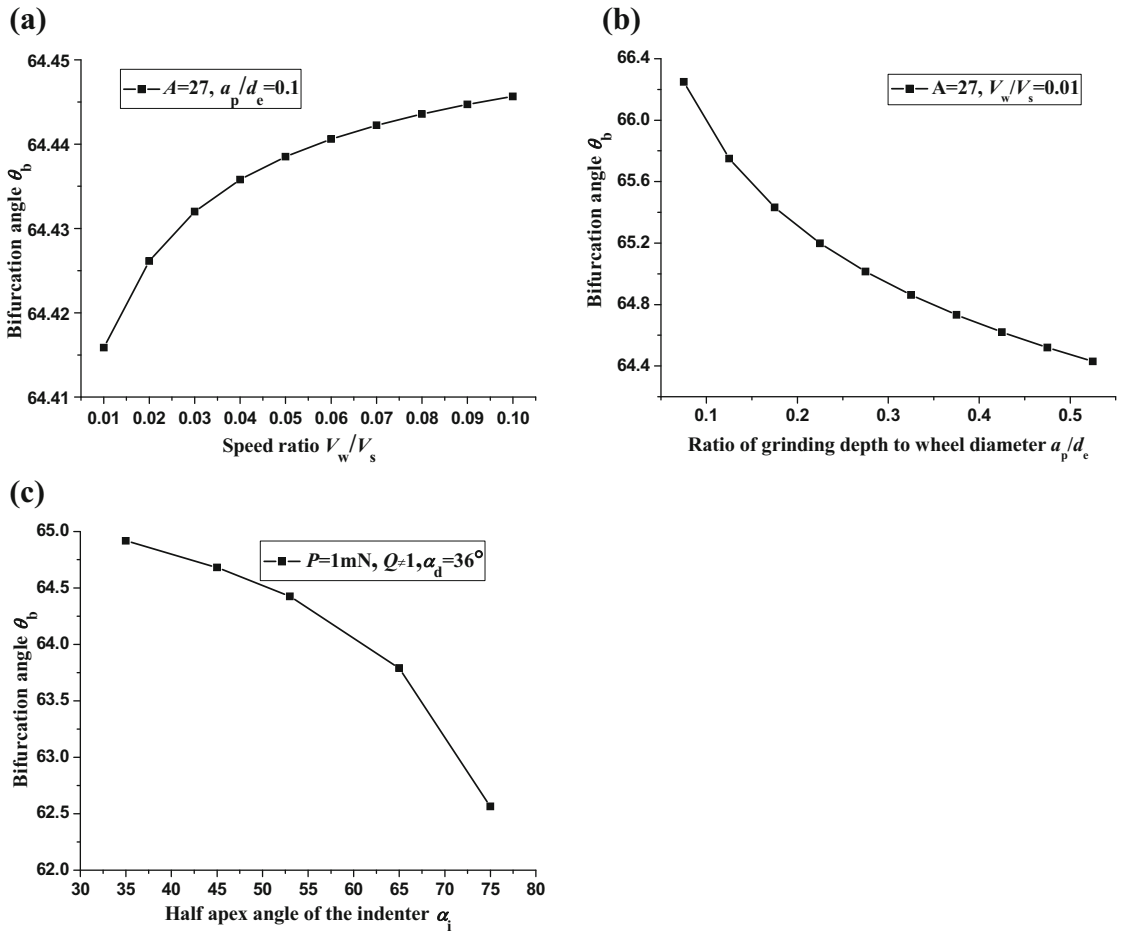

Fig. 8 Bifurcation angle at various **a** speed ratio, **b** grinding depth, **c** indenter's apex angle

providing an example of crack bifurcation after nucleation. In the following analysis, the bifurcation angle θ_b is calculated as Eq. (51) according to Erdogan's criterion mentioned by Chang et al. [64].

$$\tan\left(\frac{\theta_b}{2}\right) = \frac{1}{4}\left(\frac{K_I}{K_{II}}\right) \pm \frac{1}{4}\sqrt{\left(\frac{K_I}{K_{II}}\right)^2 + 8} \tag{51}$$

The effects of grinding speed, grinding depth and the apex of indenter on bifurcation angle are shown in Fig. 8. Results indicate that the large grinding depth and the large apex angel of indenter will increase the bifurcation angle, while the grinding depth has little effect on it. In particular, the calculated bifurcation angle is approximately between 62.5° and 66.5°. Therefore, the result is within the acceptable range of values.

5 Conclusions

As one of the most significant properties of brittle materials, the estimation of subsurface crack propagation resistance in finish machining has been drawn much attention. However, controlling the crack stability is still a challenge. In this paper, the grinding of brittle materials with pre-existing subsurface crack is analyzed utilizing a numerical investigation of stress intensity factor (SIF) from the perspective of process parameters. Both the plastic deformation below the tool and the intrinsic line defect (dislocation) located at the plastic zone boundary in silicon substrate are taken into consideration. This analysis aims at understanding the influence of various grinding parameters and tool geometries on the growth of subsurface crack. The results can be used to provide guidance for the development of controlled spalling technology which enables the reuse of cracking substrate. The conclusions drawn from this study are:

1. The main fracture mode for median crack induced in brittle material is opening rather than shear. A large compressive force perpendicular to surface will promote the growth of type I cracking and make the occurrence of mode II crack difficult. Comparing with the situation in the presence of lateral force, the threshold normal force of fracture occurrence is much larger when the lateral force is zero. It indicates that the residual stress caused by plastic zone plays an important role in fracture behavior.
2. A single edge dislocation at plastic zone boundary can bring about 3 % of mode I SIF when normal force is close to 10 mN. Since a high dislocation density may exhibit around the potential crack, the effect of dislocations on fracture behavior cannot be ignored in machining of brittle crystal materials. In addition, the edge dislocation generates a positive mode II SIF, while the lateral force induces a negative one. The mode II SIF is totally caused by the combination of dislocation and residual stress.
3. As a main fracture mode in brittle crystal materials grinding, the starting point of opening fracture is also affected by grinding parameters and tool geometry. A small grinding speed, a sharp large tool, a large table speed and grinding depth will lead to strong anti-shielding effect on mode I crack propagation and strong shielding effect on mode II crack propagation.

Acknowledgements The authors would like to deeply appreciate the support from the NNSFC (51601100, 11672141, 11572118 and 11402128), the Hunan Provincial Science Fund for Distinguished Young Scholars (2015JJ1006), the Fok Ying-Tong Education Foundation, China (141005), and K. C. Wong Magna Fund administered by Ningbo University.

References

1. Darder, M., Aranda, P., Ruiz-Hitzky, E.: Bionanocomposites: a new concept of ecological, bioinspired, and functional hybrid materials. Adv. Mater. **19**, 1309–1319 (2007)
2. Venkatachalam, S., Li, X.P., Liang, S.Y.: Predictive modeling of transition undeformed chip thickness in ductile-regime micro-machining of single crystal brittle materials. J. Mater. Process. Tech. **209**, 3306–3319 (2009)
3. Garcia, A.P., Buehler, M.J.: Bioinspired nanoporous silicon provides great toughness at great deformability. Comput. Mater. Sci. **48**, 303–309 (2010)
4. Arif, M., Zhang, X.Q., Rahman, M., Kumar, S.: A predictive model of the critical undeformed chip thickness for ductile-brittle transition in nano-machining of brittle materials. Int. J. Mach. Tool Manuf. **64**, 114–122 (2013)
5. Lawn, B.R.: Fracture of Brittle Solids. Cambridge University Press, London (1993)
6. Chen, J.B., Fang, Q.H., Li, P.: Effect of grinding wheel spindle vibration on surface roughness and subsurface damage in brittle material grinding. Int. J. Mach. Tool Manuf. **91**, 12–23 (2015)
7. Cook, J., Gordon, J.E., Evans, C.C., Marsh, D.M.: A mechanism for the control of crack propagation in all-brittle systems. Proc. R. Soc. Lond. Ser. A: Math. Phys. Sci. **282**, 508–520 (1964)
8. Hillberry, B.M., Myers, R.J.: Method for fracturing crystalline materials. US Patent 3,901,423 [P]. U.S. Patent and Trademark Office, Washington (1975)
9. Ewart, L., Suresh, S.: Crack propagation in ceramics under cyclic loads. J. Mater. Sci. **22**, 1173–1192 (1987)
10. Xu, X.P., Needleman, A.: Numerical simulations of fast crack growth in brittle solids. J. Mech. Phys. Solids **42**, 1397–1434 (1994)
11. Gao, H.J., Huang, Y.G., Abraham, F.F.: Continuum and atomistic studies of intersonic crack propagation. J. Mech. Phys. Solids **49**, 2113–2132 (2001)

12. Aslan, O., Cordero, N.M., Gaubert, A., Forest, S.: Micromorphic approach to single crystal plasticity and damage. Int. J. Eng. Sci. **49**, 1311–1325 (2011)
13. Bouchard, P.O., Bernacki, M., Parks, D.M.: Analysis of stress intensity factors and T-stress to control crack propagation for kerf-less spalling of single crystal silicon foils. Comput. Mater. Sci. **69**, 243–250 (2011)
14. Yu, T.X., Yang, J.L., Reid, S.R.: Dynamic behaviour of elastic-plastic free-free beams subjected to impulsive loading. Int. J. Solids Struct. **33**, 2659–2680 (1996)
15. Yu, T.X., Chen, F.L.: A further study of plastic shear failure of impulsively loaded clamped beams. Int. J. Impact Eng. **24**, 613–629 (2000)
16. Huang, X., Lu, G., Yu, T.X.: On the axial splitting and curling of circular metal tubes. Int. J. Mech. Sci. **44**, 2369–2391 (2002)
17. Comninou, M., Schmueser, D., Dundurs, J.: Frictional slip between a layer and substrate caused by a normal load. Int. J. Eng. Sci. **18**, 131–137 (1980)
18. Comninou, M., Barber, J.R., Dundurs, J.: Interface slip caused by a surface load moving at constant speed. Int. J. Mech. Sci. **45**, 41–46 (1983)
19. Cai, Y., Zhuang, X., Zhu, H.: A generalized and efficient method for finite cover generation in the numerical manifold method. Int. J. Comput. Methods **10**, 1350028 (2013)
20. Zhuang, X., Augarde, C., Mathisen, K.: Fracture modeling using meshless methods and level sets in 3D: framework and modeling. Int. J. Numer. Methods Eng. **92**, 969–998 (2012)
21. Petucci, J., LeBlond, C., Karimi, M.: Molecular dynamics simulations of brittle fracture in fcc crystalline materials in the presence of defects. Comput. Mater. Sci. **86**, 130–139 (2014)
22. Lawn, B.R.: Atomically sharp cracks in brittle solids: an electron microscopy study. J. Mater. Sci. **15**, 1207–1223 (1980)
23. Rice, J.R., Thomson, R.: Ductile versus brittle behaviour of crystals. Philos. Mag. **29**, 73 (1974)
24. Inamura, T., Shimada, S., Takezawa, N., Nakahara, N.: Brittle/ductile transition phenomena observed in computer simulations of machining defect-free monocrystalline silicon. CIRP Ann. Manuf. Tech. **46**, 31–34 (1997)
25. Beltz, G.E., Lipkin, D.M., Fischer, L.L.: Role of crack blunting in ductile versus brittle response of crystalline materials. Phys. Rev. Lett. **82**, 4468 (1999)
26. Fischer, L.L., Beltz, G.E.: The effect of crack blunting on the competition between dislocation nucleation and cleavage. J. Mech. Phys. Solids **49**, 635–654 (2001)
27. Deshpande, V.S., Needleman, A., Van der Giessen, E.: Discrete dislocation modeling of fatigue crack propagation. Acta Mater. **50**, 831–846 (2002)
28. Cleveringa, H.H.M., Van der Giessen, E., Needleman, A.: A discrete dislocation analysis of mode I crack growth. J. Mech. Phys. Solids **48**, 1133–1157 (2000)
29. Frederiksen, T., Brandbyge, M., Lorente, N., Jauho, A.P.: Inelastic scattering and local heating in atomic gold wires. Phys. Rev. Lett. **93**, 256601 (2004)
30. Sen, D., Thaulow, C., Schieffer, S.V., Cohen, A., Buehler, M.J.: Atomistic study of crack-tip cleavage to dislocation emission transition in silicon single crystals. Phys. Rev. Lett. **104**, 235502 (2010)
31. Zhou, K., Nazarov, A.A., Wu, M.S.: Continuum and atomistic studies of a disclinated crack in a bicrystalline nanowire. Phys. Rev. B **73**, 045410-1–045410-11 (2006)
32. Zhou, K., Wu, M.S., Nazarov, A.A.: Relaxation of a disclinated tricrystalline nanowire. Acta Mater. **56**, 5828–5836 (2008)
33. Zhou, K., Wei, R.B.: Modeling cracks and inclusions near surfaces under contact loading. Int. J. Mech. Sci. **83**, 163–171 (2014)
34. Fang, Q.H., Liu, Y.W., Jiang, C.P.: Edge dislocation interacting with an interfacial crack along a circular inhomogeneity. Int. J. Solids Struct. **40**, 5781–5797 (2003)
35. Fang, Q.H., Liu, Y.W., Jiang, C.P., Li, B.: Interaction of a wedge disclination dipole with interfacial cracks. Eng. Fract. Mech. **73**, 1235–1248 (2006)
36. Fang, Q.H., Liu, Y., Liu, Y.W., Huang, B.Y.: Dislocation emission from an elliptically blunted crack tip with surface effects. Phys. B **404**, 3421–3424 (2009)
37. Broese van Groenou, A., Veldkamp, D.B.: Grinding brittle materials. Philips Tech. Rev. **38**, 105–118 (1979)
38. Toh, S.B., McPherson, R.: Fine scale abrasive wear of ceramics by a plastic cutting process. In: Almond, E.A., Brookes, C.A., Warren, R. (eds.) Proceedings of Second International Conference on Science of Hard Materials held at Rhodes 23–28 Sept 1984. Adam Hilger, Bristol. pp. 865 (1986)
39. Moore, M.A., King, F.S.: Abrasive wear of brittle solids. Wear **60**, 123 (1980)
40. Lawn, B., Wilshaw, R.: Indentation fracture: principles and applications. J. Mater. Sci. **10**, 1049 (1975)
41. Nakamura, M., Sumomogi, T., Endo, T.: Evaluation of surface and subsurface cracks on nano-scale machined brittle materials by scanning force microscope and scanning laser microscope. Surf. Coat. Technol. **169–170**, 743–747 (2003)
42. Yan, J.W., Zhang, Z.Y., Kuriyagawa, T.: Mechanism for material removal in diamond turning of reaction-bonded silicon carbide. Int. J. Mach. Tool Manuf. **49**, 366–374 (2009)
43. Wang, M.H., Wang, W., Lu, Z.S.: Critical cutting thickness in ultra-precision machining of single crystal silicon. Int. J. Adv. Manuf. Technol. **65**, 843–851 (2013)
44. Kharin, V.S., Zakharov, M., Bulatova, A.: Nucleation and growth of microcracks: an improved dislocational model and implications for ductile/brittle behaviour analysis. EGF9 (2013)
45. Kachanov, M., Karpetian, E.: Three-dimensional interactions of a half-plane crack with point forces, dipoles and moments. Int. J. Solids Struct. **34**, 4101–4125 (1997)
46. Kiris, A., Kachanov, M.: Contacts and cracks of complex shapes: crack-contact dualities and relations between normal and shear compliances. Int. J. Eng. Sci. **50**, 233–255 (2012)
47. Zhao, Y.X., Fang, Q.H., Liu, Y.W., Jiang, C.Z.: Shielding effects of disclinations on the elliptical blunt crack. Int. J. Eng. Sci. **70**, 91–101 (2013)
48. Fang, Q.H., Zhang, L.C.: Prediction of the threshold load of dislocation emission in silicon during nanoscratching. Acta Mater. **61**, 5469–5476 (2013)

49. Fang, Q.H., Zhang, L.C.: Emission of partial dislocations in silicon under nanoindentation. J. Mater. Res. **28**, 1995–2003 (2013)
50. Bernstein, N., Hess, D.W.: Lattice trapping barriers to brittle fracture. Phys. Rev. Lett. **91**, 025501 (2003)
51. Deegan, R.D., Chheda, S., Patel, L., Marder, M., Swinney, H.L., Kim, J., et al.: Wavy and rough cracks in silicon. Phys. Rev. E **67**, 066209 (2003)
52. Malkin, S., Hwang, T.W.: Grinding mechanisms for ceramics. Ann. CIRP **45**, 569–580 (1996)
53. Lawn, B.R., Evans, A.G.: A model for crack initiation in elastic/plastic indentation fields. J. Mater. Sci. **12**, 2195–2199 (1977)
54. Lambropoulos, J.C., Jacobs, S.D., Ruckman, J.: Material removal mechanisms from grinding to polishing. Ceram. Trans. **102**, 113–128 (1999)
55. Jing, X.N., Maiti, S., Subhash, G.: A new analytical model for estimation of scratch-induced damage in brittle solids. J. Am. Ceram. Soc. **90**, 885–892 (2007)
56. Lawn, B.R., Evans, A.G., Marshall, D.B.: Elastic/plastic indentation damage in ceramics: the median/radial crack system. J. Am. Ceram. Soc. **63**, 574–581 (1980)
57. Johnson, K.L.: Contact Mechanics. Cambridge University Press, London (1985)
58. Ahn, Y., Farris, T.N., Chandrasekar, S.: Sliding microindentation fracture of brittle materials: role of elastic stress fields. Mech. Mater. **29**, 143–152 (1998)
59. Hills, D.A., Kelly, P.A.: Solution of Crack Problems: The Distributed Dislocation Technique. Kluwer Academic Publishers, Dordecht (1996)
60. Erdogan, F., Gupta, G.D.: On the numerical solution of singular integral equations. Q. Appl. Math. **29**, 525–534 (1972)
61. Dundurs, J., Comninou, M.: Some consequences of the inequality conditions in contact and crack problems. J. Elast. **9**, 71–82 (1979)
62. Chen, J.B., Fang, Q.H., Liu, Y.W.: Interaction between dislocation and subsurface crack under condition of slip caused by half-plane contact surface normal force. Eng. Fract. Mech. **114**, 115–126 (2013)
63. Chen, X., Rowe, W.B., McCormack, D.F.: Analysis of the transitional temperature for tensile residual stress in grinding. J. Mater. Process. Tech. **107**, 216–221 (2000)
64. Chang, J., Xu, J.Q., Mutoh, Y.: A general mixed-mode brittle fracture criterion for cracked materials. Eng. Fract. Mech. **73**, 1249–1263 (2006)
65. Yan, J., Asami, T., Harada, H., Kuriyagawa, T.: Fundamental investigation of subsurface damage in single crystalline silicon caused by diamond machining. Precis. Eng. **33**, 378–386 (2009)
66. Zhu, D.H., Yan, S.J., Li, B.Z.: Single-grit modeling and simulation of crack initiation and propagation in SiC grinding using maximum undeformed chip thickness. Comput. Mater. Sci. **92**, 13–21 (2014)
67. Gu, W.B., Yao, Z.: Evaluation of surface cracking in micron and sub-micron scale scratch tests for optical glass BK7. J. Mech. Sci. Tech. **25**, 1167–1174 (2011)
68. Shaw, M.: Principles of Abrasive Processing. Oxford University Press, Oxford (1996)
69. Li, X.Z., Nakano, M., Yamauchi, Y., Kishida, K., Tanaka, K.A.: Microcracks, spall and fracture in glass: a study using short pulsed laser shock waves. J. Appl. Phys. **83**, 3583 (1998)
70. Kozhushko, V.V., Hess, P.: Comparison of mode-resolved fracture strength of silicon with mixed-mode failure of diamond crystals. Eng. Fract. Mech. **77**, 193–200 (2010)